In situ genetic engineering of tumors for long-lasting and systemic immunotherapy

Stephany Y. Tzeng[a,b,c], Kisha K. Patel[a,b,c], David R. Wilson[a,b,c], Randall A. Meyer[a,b,c], Kelly R. Rhodes[a,b,c], and Jordan J. Green[a,b,c,d,e,f,g,h,i,1]

[a]Department of Biomedical Engineering, Johns Hopkins School of Medicine, Baltimore, MD 21218; [b]Translational Tissue Engineering Center, Johns Hopkins School of Medicine, Baltimore, MD 21231; [c]Institute for NanoBioTechnology, Johns Hopkins University, Baltimore, MD 21218; [d]Department of Oncology, Johns Hopkins School of Medicine, Baltimore, MD 21218; [e]Department of Materials Science and Engineering, Johns Hopkins University, Baltimore, MD 21218; [f]Department of Chemical and Biomolecular Engineering, Johns Hopkins University, Baltimore, MD 21218; [g]Department of Neurosurgery, Johns Hopkins School of Medicine, Baltimore, MD 21218; [h]Department of Ophthalmology, Johns Hopkins School of Medicine, Baltimore, MD 21287; and [i]Bloomberg-Kimmel Institute for Cancer Immunotherapy, Sidney Kimmel Comprehensive Cancer Center, Johns Hopkins School of Medicine, Baltimore, MD 21231

Edited by Kristi S. Anseth, University of Colorado Boulder, Boulder, CO, and approved January 15, 2020 (received for review September 15, 2019)

Cancer immunotherapy has been the subject of extensive research, but highly effective and broadly applicable methods remain elusive. Moreover, a general approach to engender endogenous patient-specific cellular therapy, without the need for a priori knowledge of tumor antigen, ex vivo cellular manipulation, or cellular manufacture, could dramatically reduce costs and broaden accessibility. Here, we describe a biotechnology based on synthetic, biodegradable nanoparticles that can genetically reprogram cancer cells and their microenvironment in situ so that the cancer cells can act as tumor-associated antigen-presenting cells (tAPCs) by inducing coexpression of a costimulatory molecule (4-1BBL) and immunostimulatory cytokine (IL-12). In B16-F10 melanoma and MC38 colorectal carcinoma mouse models, reprogramming nanoparticles in combination with checkpoint blockade significantly reduced tumor growth over time and, in some cases, cleared the tumor, leading to long-term survivors that were then resistant to the formation of new tumors upon rechallenge at a distant site. In vitro and in vivo analyses confirmed that locally delivered tAPC-reprogramming nanoparticles led to a significant cell-mediated cytotoxic immune response with systemic effects. The systemic tumor-specific and cell-mediated immunotherapy response was achieved without requiring a priori knowledge of tumor-expressed antigens and reflects the translational potential of this nanomedicine.

cancer | immunotherapy | nanoparticles | nonviral | gene delivery

Immunotherapy has been used successfully in the clinic to treat certain cancers that do not respond to conventional treatment (1). A critical goal of immunotherapy is the activation of a cell-mediated immune response that can specifically kill tumor cells (2). Under ideal circumstances, a cytotoxic antitumor response could be generated via coordinated signaling between antigen-presenting cells (APCs) and $CD8^+$ T cells. Signals important for T cell activation include signal 1, the tumor antigen in the context of major histocompatibility complex (MHC) class I; signal 2, surface-bound costimulatory molecules (3); and signal 3, secreted immunostimulatory cytokines that contribute to cell recruitment and differentiation (4).

Engineering of a patient's natural APCs to enhance this interaction is often constrained by high costs and safety risks of ex vivo cell manipulation (5–7) or the technical challenges of targeted in situ APC manipulation (7, 8). The use of artificial APCs (aAPCs) (9, 10), generally composed of biomimetic synthetic particles, often still requires ex vivo cell manipulation (6), and the production of tumor- and patient-specific antigen:MHC complexes for aAPC manufacturing is inefficient. Further, the best antigens to use in a given setting are unclear, vary between patients, and require a priori knowledge before treatment, and tumor neoantigen identification remains a major challenge in the field, as well as being limited in its applicability to different patients (11). Additionally, cancer cells avoid immune surveillance using several strategies, such as the often unpredictable variability in tumor antigen expression, as well as the expression of immunosuppressive signals by tumor cells. The heterogeneous tumor environment therefore limits the efficacy of targeting single tumor-associated antigens via aAPCs or delivery of specific tumor antigens as vaccines (12, 13).

In this report, we describe an in situ vaccination strategy that takes advantage of the intrinsic expression of signal 1 (antigen:MHC) by many tumor cells (14), allowing the technology itself to remain antigen-agnostic, not requiring a priori knowledge of potential neoantigens. Tumor cells are engineered directly in vivo by safe synthetic, biodegradable gene-delivery nanoparticles composed of poly(beta-amino ester)s (PBAEs), which induce simultaneous expression of the costimulatory molecule 4-1BBL (signal 2) (15, 16) and the secreted cytokine IL-12 (signal 3) (17, 18). 4-1BBL has been shown to bias the immune system toward a $CD8^+$ T cell-driven cytotoxic response (15, 16) and to stimulate other components of the immune system, including natural killer (NK) cells and APCs (19). IL-12 is also known to promote NK cell activity (18, 20), which is particularly important in the case of tumor cells that downregulate MHC I expression to avoid immune surveillance. The resulting coexpression of signals 1, 2, and 3 reprograms tumor cells and their microenvironment into what we term "tumor-associated APCs" (tAPCs).

Significance

There is an urgent need for improved cancer immunotherapies. The nanoparticles described here deliver genes to stimulate the immune system to specifically kill tumor cells. This synthetic, biodegradable system avoids the use of common gene delivery materials like viruses that can have safety concerns and manufacturing limitations. Local nanoparticle delivery evades adverse side effects stemming from systemic administration of immune-activating therapeutics. Importantly, this technology causes a tumor-targeting response but does not require prior knowledge of a particular patient's gene expression profile; thus, it can serve as a platform to combat many different solid cancers. Moreover, local nanoparticle administration causes a systemic cellular immune response, which has the potential to lead to better outcomes in the context of recurrence or metastasis.

Author contributions: S.Y.T., D.R.W., R.A.M., and J.J.G. designed research; S.Y.T. and K.K.P. performed research; S.Y.T. and K.R.R. analyzed data; and S.Y.T. and J.J.G. wrote the paper.

Competing interest statement: J.J.G., R.A.M., S.Y.T., and D.R.W. disclose inventorship on patent filings related to this manuscript filed by Johns Hopkins University.

This article is a PNAS Direct Submission.

[1]To whom correspondence may be addressed. Email: green@jhu.edu.

This article contains supporting information online at https://www.pnas.org/lookup/suppl/doi:10.1073/pnas.1916039117/-/DCSupplemental.

First published February 7, 2020.

The delivery or expression of soluble cytokines (21–23) or adjuvants (24, 25), either systemically or locally, has been reported, as has the delivery of immunostimulatory agents to elicit responses from natural professional APCs (24, 26, 27). These studies highlight the potential of engineering the microenvironment with biological molecules to enhance cellular immune responses. However, in our distinctive approach, we deliver a biodegradable nonviral nanoparticle that induces the overexpression of both signals 2 and 3 on signal 1-bearing tumor cells. This directly activates T cells in the context of the tumor antigen, leading to an antigen-specific cellular response despite the antigen-free technology. Local expression of these immune-stimulatory molecules is crucial: Systemic delivery of signal 2 agonists and cytokines can cause adverse side effects (28–30) while the improved function of CAR-T cells expressing signal 2 underscores the importance of costimulation as a part of immunotherapies (31). Local gene delivery to overexpress cytokines and costimulatory signal 2 in the tumor itself is therefore a promising strategy to address this issue. Further, while conventional virus-based delivery can be effective for in vivo gene transfer (32), here, we use biodegradable PBAE-based nanoparticles (NPs), utilizing a nonviral biotechnology to deliver DNA to cancer cells with high efficacy and specificity over healthy tissue (33, 34). Notably, this approach avoids the intrinsic immunogenicity or toxicity of more traditional gene transfer vectors like viruses and lipid nanoparticles (35, 36), while also facilitating large and flexible DNA cargo carrying capacity.

Here, we test the tAPC reprogramming strategy in a B16-F10 murine model of melanoma, which is challenging to treat by immunotherapy. We show the strong effect of PBAE-based nanoparticles carrying *4-1BBL* and *IL-12* DNA, particularly in combination with anti–PD-1 checkpoint blockade therapy, on tumor growth and animal survival. We also explore the mechanism of action of this technology using in vitro and in vivo assays to quantify the effects of tAPC reprogramming on the local and systemic immune system. Finally, we show that these results can be replicated in a second tumor, the MC38 colorectal carcinoma model, supporting the potential clinical utility of the technology.

Results

Selection of PBAE Transfection Agent for B16-F10 Cells In Vitro and In Vivo. An array of PBAEs were synthesized based on structures previously shown to be safe and effective at transfecting various types of cancer cells with specificity over healthy cells (33, 34, 37) (Fig. 1*A*). B16-F10 cells were transfected in vitro with green fluorescent protein (*GFP*) DNA as a reporter gene to assess gene transfer efficacy. Among the nanoparticle formulations with low (<20%) toxicity, the top three polymers, named 4-4-7, 4-4-27, and 5-3-49, transfected 93.0 ± 0.6%, 88.6 ± 0.4%, and 88 ± 2% of cells, respectively (Fig. 1 *B* and *C*), with geometric mean fluorescence intensities of 440 ± 40-, 350 ± 50-, and 260 ± 50-fold above the untreated control, respectively (*SI Appendix*, Fig. S1).

The top three PBAEs were then used to form nanoparticles with firefly luciferase (*fLuc*) DNA for in vivo transfection of subcutaneous (s.c.) B16-F10 tumors. After intratumoral (i.t.) injection of 5 μg of *fLuc* DNA in PBAE nanoparticles, the In Vivo Imaging System (IVIS) was used to measure gene expression in the tumor (Fig. 1 *D* and *E*). PBAEs 4-4-7, 4-4-27, and 5-3-49 led to 11 ± 9-, 22 ± 5-, and 6 ± 5-fold higher luminescence signal than control animals, and PBAE 5-3-49 was selected as the lead in vivo transfection agent for all further in vitro or in vivo studies on delivery of functional genes. Transmission electron microscopy (TEM) imaging showed that nanoparticles are ∼50 to 100 nm when dry, and nanoparticle tracking analysis (NTA) and dynamic light scattering (DLS) measured a number-average hydrodynamic diameter of 143 ± 6 nm and an intensity-weighted Z-average hydrodynamic diameter of 231 ± 3 nm, respectively (Fig. 1*F*). As expected, due to a large ratio of cationic polymer to anionic DNA, nanoparticles were measured by electrophoretic motility to have a positive zeta potential of approximately +23.3 ± 0.9 mV.

In Vitro Expression of 4-1BBL and IL-12 by Transfected B16-F10 Cells. Using PBAE 5-3-49, B16-F10 cells were transfected in vitro with both *4-1BBL* and *IL-12*, evaluating various ratios of the two plasmids. The supernatant was collected after 24 and 48 h and measured by conformational enzyme-linked immunosorbent assay (ELISA) for IL-12 expression (Fig. 2*A*). IL-12 was detected

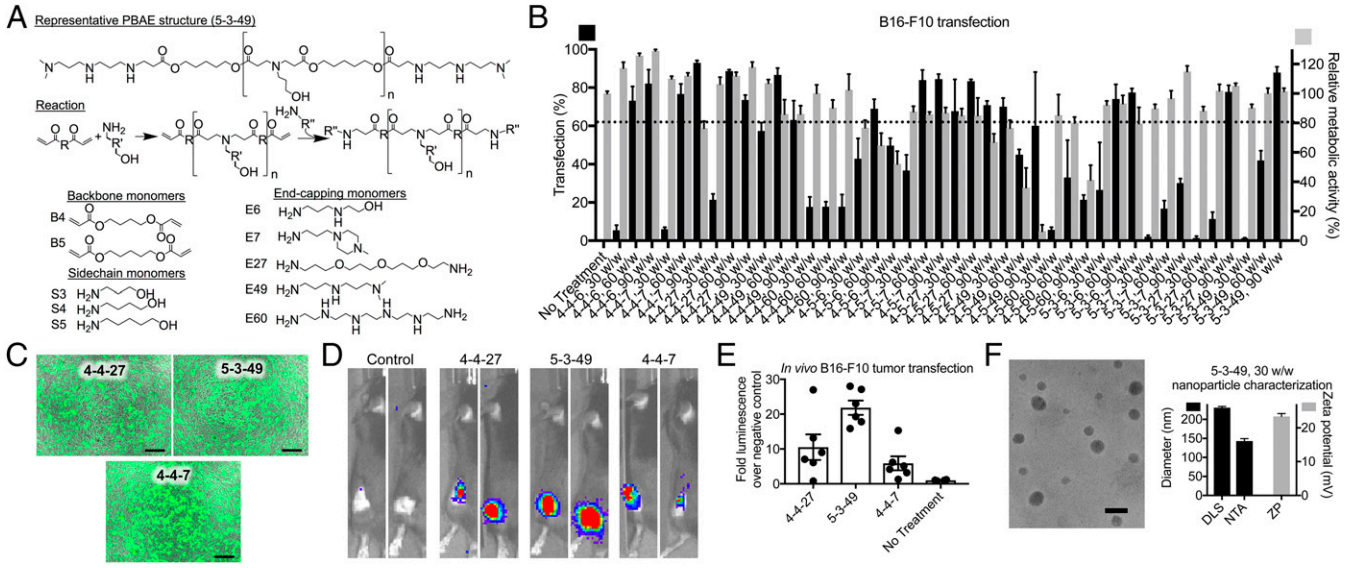

Fig. 1. PBAE nanoparticles transfect B16-F10 melanoma cells with reporter genes in vitro and in vivo. (*A*) Monomers used to synthesize PBAEs are shown. (*B*) PBAE nanoparticles were used to transfect B16-F10 cells with GFP DNA using varying mass ratios (w/w) of PBAE to DNA. Mean ± SE are shown ($n = 4$). (*C*) Fluorescence micrographs were taken of the leading formulations. (Scale bars: 200 μm.) (*D* and *E*) subcutaneous tumors in C57BL/6 mice were transfected with fLuc using leading nanoparticles and imaged by IVIS after 24 h. Mean ± SE are shown ($n = 4$ for control; $n = 6$ for all other groups). (*F*) TEM was used to visualize the nanoparticles. (Scale bar: 100 nm.) DLS and NTA were used to measure size, and electrophoretic mobility was used to measure zeta potential (ZP). Mean ± SE are shown ($n = 3$).

by ELISA at both time points, with the most cytokine released within the first 24 h of transfection and ∼50% less being released over the following 24 h. As expected, the amount of secreted IL-12 was tunable based on the *4-1BBL:IL-12* plasmid ratio, but, at all ratios tested, high IL-12 levels were detectable by ELISA. Expression of surface-bound 4-1BBL was measured by flow cytometry and was detected on transfected B16-F10 cells (Fig. 2 *B* and *C*), with an increasing proportion of cells transfected (% 4-1BBL$^+$) and increasing amount of protein produced (normalized fluorescence intensity) as the ratio of *4-1BBL:IL-12* increased.

Even at a 50:50 mass ratio of the two plasmids, 62 ± 10% of cells were 4-1BBL$^+$. In this condition, a total of 69 ± 10 ng/mL IL-12 was also secreted over 48 h, corresponding to 69 ± 10 ng from a starting number of 10^5 cells, an amount that surpasses concentrations shown to induce Th1 differentiation or expansion of cytotoxic T cells (38). These results indicate the feasibility of cocomplexing and codelivering both plasmids at once to convert B16-F10 cells into tAPCs.

In Vitro Activation of Cytotoxic Lymphocytes by B16-F10 tAPCs. As a demonstration of the feasibility of this strategy for immune stimulation, B16-F10 cells were transfected in vitro with *4-1BBL* and/or *IL-12* to reprogram them into tAPCs. The tAPCs were then cocultured with primary CD8$^+$ T cells or NK cells isolated from the spleens of C57BL/6 mice. After 18 h, the concentration of secreted interferon (IFN)-γ in the culture medium was measured by ELISA as a surrogate for T or NK cell activation (Fig. 2*D*). B16-F10 cells transfected with a control plasmid (*fLuc*) or with *4-1BBL* alone elicited nearly undetectable levels of IFN-γ expression. Transfection with *IL-12* alone elicited significantly higher but still low amounts of IFN-γ secretion, compared with the control. However, transfection with both *4-1BBL* and *IL-12* in combination showed strong synergy between the two signals, resulting in significantly greater IFN-γ secretion than the additive effect of the two genes on their own. Similar patterns were seen with both CD8$^+$ T cells and NK cells, suggesting that this combination of signals 2 and 3 is suitable for activation of both types of cytotoxic immune cells.

To more quantitatively assess the synergy between signals 2 and 3, B16-F10 cells were transfected in vitro with a wide range of doses of *4-1BBL* alone, *IL-12* alone, or combinations of the *4-1BBL* and *IL-12* plasmids at 1:3, 1:1, and 3:1 plasmid mass ratios. After coculture with primary CD8$^+$ T cells, it was found that signals 2 and 3 alone are unable to strongly stimulate IFN-γ secretion, even at the highest doses tested, while treatment with the plasmid combinations resulted in the expected dose–response of IFN-γ secretion (Fig. 2*E*). When the effects (IFN-γ secretion) of *4-1BBL* transfection alone and *IL-12* transfection alone were added together, it was found that the effect of transfection with a matched total plasmid dose of *4-1BBL* and *IL-12* in combination was statistically significantly higher starting at a dose of 50 ng of plasmid per well for some combinations, and all combinations were significantly higher than the added effects of transfection with the individual plasmids at higher doses (Fig. 2*F*).

In Situ Genetic Reprogramming of B16-F10 Tumors for Anticancer Immunotherapy. B16-F10 melanoma cells were inoculated s.c. in the flank of C57BL/6 mice. PBAE/DNA nanoparticles were injected i.t. on days 7, 9, and 11 after tumor inoculation, and anti–PD-1 monoclonal antibody was administered intraperitoneally (i.p.) on days 7 and 9. On day 14, 3 d after the final nanoparticle treatment, IFN-γ was measured in the tumor interstitial fluid (TIF) by ELISA in tumors treated with signal 2 and/or 3 nanoparticles (Fig. 3*A*). Results followed a similar trend to that seen in vitro, with IL-12 having a stronger effect than 4-1BBL alone and the combination of both signals 2 and 3 eliciting the greatest amount of IFN-γ secretion. Interestingly, although anti–PD-1 administration alone was not sufficient to elicit IFN-γ secretion, mice treated with both 4-1BBL/IL-12 nanoparticles and anti–PD-1 together had greater IFN-γ in the TIF than mice treated with nanoparticles alone.

The tumors in mice treated with anti–PD-1 and control (fLuc) nanoparticles grew similarly (no statistically significant differences) to the tumors in mice treated with control nanoparticles alone (*SI Appendix*, Fig. S2). Among mice treated with anti–PD-1 in the background, a gold-standard immunotherapy used in the clinic for advanced melanoma, tumor growth was significantly

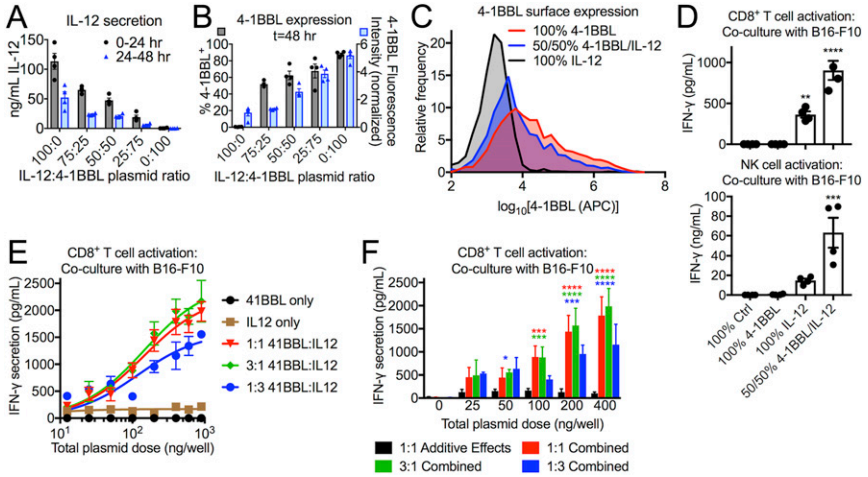

Fig. 2. B16-F10 melanoma cells transfected to express signals 2 and 3 in vitro cause activation of primary T and NK cells. (*A*–*C*) B16-F10 cells were transfected with 5-3-49 PBAE/DNA nanoparticles encoding IL-12, 4-1BBL, or both. Secreted IL-12 was measured by ELISA, and surface-bound 4-1BBL was measured by flow cytometry. (*D*) Transfection with a mixture of the 4-1BBL and IL-12 plasmids results in a synergistic effect greater than the additive effects of each plasmid on its own. (*E* and *F*) Across different doses of total plasmid per well, the effect (IFN-γ secretion) of 4-1BBL and IL-12 plasmids in combination is consistently higher than the added effects of 4-1BBL transfection alone and IL-12 transfection alone. For *A*–*D*, statistically significant differences were measured by one-way ANOVA with Dunnett posttests comparing to the control (100% Ctrl). All bar graphs show mean ± SE. Four ($n = 4$) replicates were used per group. For *F*, a two-way ANOVA was performed, with Dunnett posttests comparing to the control (1:1 Additive Effects). Asterisk colors correspond to the group found to be significantly different from the control at that dose. *$P < 0.05$; **$P < 0.01$; ***$P < 0.001$; ****$P < 0.0001$.

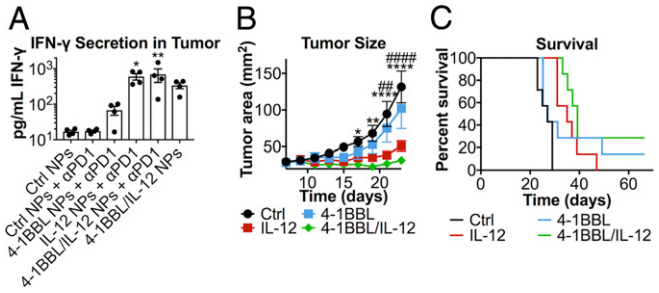

Fig. 3. In vivo tAPC reprogramming significantly inhibits tumor growth and leads to long-term survival. (*A*) IFN-γ was detectable in the tumor interstitial fluid 14 d after tumor inoculation in treated groups ($n = 4$). (*B*) Of mice treated with anti–PD-1, slower tumor growth was measured in groups treated with IL-12 nanoparticles (significance marked by #) or 4-1BBL/IL-12 nanoparticles (significance marked by *). *$P < 0.05$; ** or ##: $P < 0.01$; **** or ####: $P < 0.0001$. Significance was calculated by two-way repeated-measures ANOVA with a Dunnett posttest to compare against animals treated with control nanoparticles and anti–PD-1. (*C*) Mice treated with IL-12 or 4-1BBL/IL-12 nanoparticles and anti–PD-1 survived significantly longer than the control ($P = 0.0018$). All error bars are SEM.

slower in mice treated with IL-12 nanoparticles than in controls, and this effect was even stronger in mice treated with 4-1BBL/IL-12 nanoparticles ($P < 0.0001$ for both at t = 23 d) (Fig. 3*B*). While 4-1BBL nanoparticles did not cause significantly slower tumor growth compared to the control over the time frame analyzed, this appears to be due to large variability in the response rate for this group. This is apparent from the survival curve (Fig. 3*C*), which shows that, while the tumor in most of the mice in the 4-1BBL nanoparticle group followed similar growth trends to those seen in the controls, a small number in this group survived substantially longer—one mouse cleared the flank tumor entirely, and no disease was apparent 66 d after the initial tumor implantation in this long-term survivor. By contrast, the IL-12 nanoparticle and 4-1BBL/IL-12 nanoparticle groups (median survival of 35 d and 39 d, respectively) survived significantly ($P = 0.0018$) longer than the control group (median survival of 23 d), representing a 50 to 70% increase in median survival. A significant portion of the mice (28.6%) in the 4-1BBL/IL-12 nanoparticle group also cleared the tumor entirely and were disease-free at t = 66 d.

Analysis of Local Immune Cells In Vivo Shows Cytotoxic Cellular Responses. Tumors were excised for analysis by qPCR 10 and 14 d after tumor inoculation. Between those two time points, the relative expression of *CD45*, expressed by all leukocytes, and *CD3ε*, expressed by all T cells, decreased in the groups treated with only control nanoparticles or control nanoparticles with anti–PD-1 checkpoint blockade therapy (Fig. 4*A*). By contrast, tumors treated with tAPC reprogramming nanoparticles encoding 4-1BBL and/or IL-12 had greater expression of *CD45*, *CD3ε*,

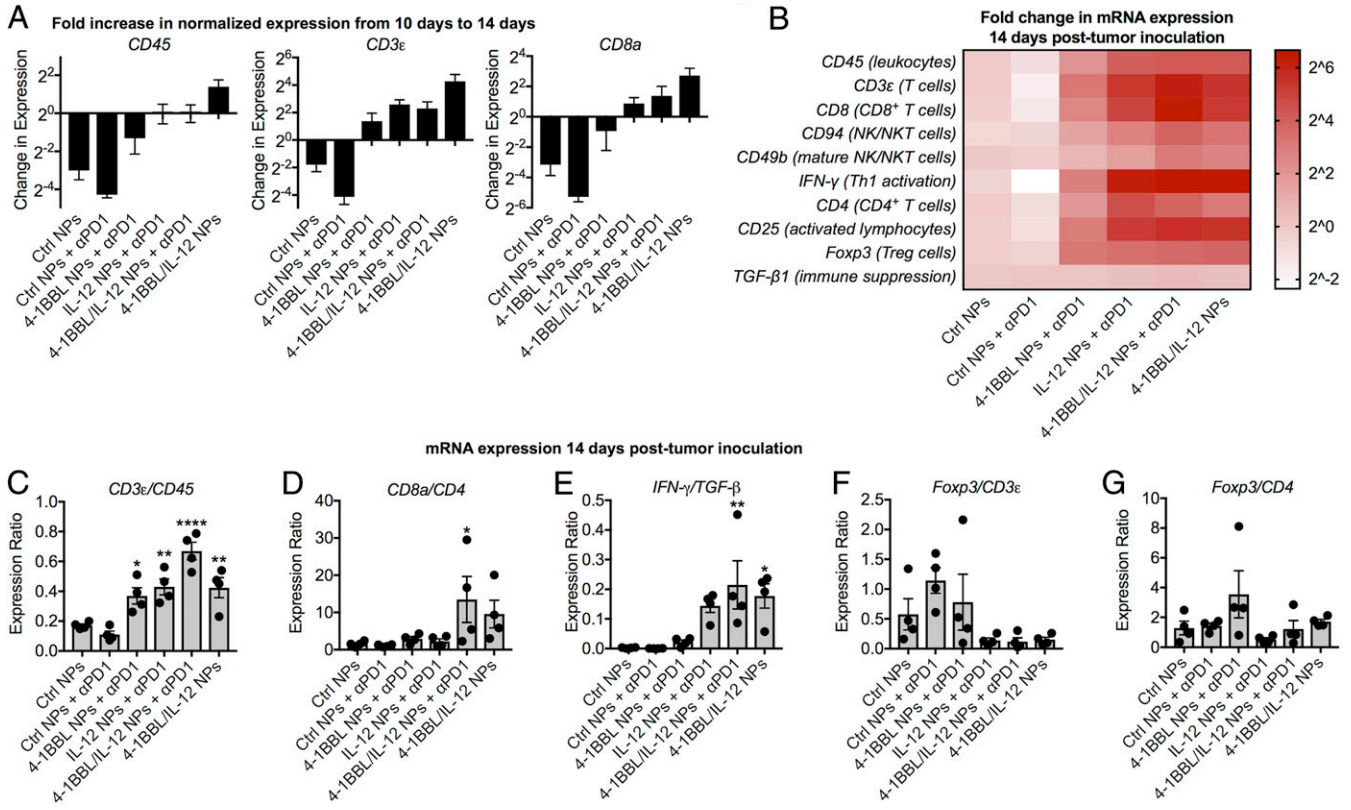

Fig. 4. Local immune cell populations measured by qPCR indicate an antitumor cytotoxic response caused by tAPC reprogramming NPs. (*A*) Genes indicating the presence of total tumor-infiltrating leukocytes, total T cells, and $CD8^+$ T cells increased between 14 and 18 d in groups that received reprogramming nanoparticles. (*B*) Treatment with signal 2 and/or 3 nanoparticles results in elevated expression of genes indicating increased proportions of infiltrating immune cells in the tumor. (*C*) Normalizing CD3ε expression to CD45 expression suggests that a greater proportion of TILs are T cells in animals treated with tAPC reprogramming nanoparticles. (*D*) The ratio of CD8a to CD4 expression suggests a more cytotoxic immune response was after treatment with tAPC-reprogramming nanoparticles. (*E*) The high ratio of IFN-γ to TGF-β expression in tAPC-treated animals suggests a bias toward Th1 antitumor activation, and (*F* and *G*) the lower ratio of Foxp3 to CD3ε and CD4 expression in those groups also suggests a decrease in Tregs at the tumor site. For all, mean ± SE of four ($n = 4$) replicates is shown. *$P < 0.05$; **$P < 0.01$; ****$P < 0.0001$; statistically significant differences were measured by one-way ANOVA with Dunnett posttests comparing to the control (Ctrl NPs).

and *CD8a* at 14 d than at 10 d. This indicates that, in the control animals, the growth of malignant tumor cells outpaced the recruitment and expansion of immune cells; the opposite appears to be the case for animals treated with reprogramming nanoparticles, with IL-12 alone or in combination with 4-1BBL having the greatest effect.

Other genes were also analyzed by qPCR after 14 d, and gene expression profiles were evaluated as an approximation of the types of immune cells present in the tumor (Fig. 4*B*). Tumor-infiltrating leukocytes (*CD45*), T cells (*CD3ε*)—particularly $CD8^+$ T cells (*CD8a*)—and NK cells (*CD94* and *CD49b*) were found to be elevated to the greatest extent in groups treated with IL-12 or 4-1BBL/IL-12 nanoparticles, either with or without additional anti–PD-1 treatment. The increase in *IFN-γ* expression in nanoparticle-treated groups followed the same trends seen via ELISA measurement of IFN-γ protein and is characteristic of a cytotoxic or Th1-biased immune response that could promote tumor control. This is in agreement with the increased expression of markers of cytotoxic lymphocytes.

Interestingly, while the overall proportion of immune cells in all nanoparticle-treated tumors appears to be higher, the ratio of *CD3ε* to *CD45* expression was highest in tumors administered 4-1BBL/IL-12 nanoparticles along with anti–PD-1, suggesting that the proportion of T cells among the infiltrating leukocytes was highest in that group (Fig. 4*C*). The ratio of *CD8a* to *CD4* expression in this group was also significantly higher, again suggesting an immune response more biased toward a Th1 or antitumor cytotoxic phenotype (Fig. 4*D*), a result corroborated by the ratio of *IFN-γ* to *TGF-β1* expression (Fig. 4*E*). Finally, while the *CD3ε* expression was elevated in 4-1BBL nanoparticle-treated groups compared to controls, measurements suggest that a greater proportion of T cells in some animals of this group have a regulatory phenotype (T regulatory cells [Tregs]), as indicated by *Foxp3* expression (Fig. 4 *F* and *G*). The ability of 4-1BB/4-1BBL signaling to induce either stimulatory or regulatory T cells under different conditions (19) may explain the large variability in results seen in mice administered nanoparticles encoding 4-1BBL alone, as some tumors in this group showed slowed growth or were eliminated entirely, while other tumors seemed to grow even more quickly than control tumors. By contrast, all of the groups treated with IL-12 or 4-1BBL/IL-12 nanoparticles showed decreased *Foxp3* expression when normalized to *CD3ε* expression, demonstrating the importance of codelivery of a Th1-biased cytokine (39). Other details of qPCR analysis on lymphocyte-related markers are provided in *SI Appendix*, Fig. S3.

Additional qPCR analysis was also carried out to investigate the effects of this therapy on components of the innate immune system and markers of the cells' activation state (*SI Appendix*, Fig. S4). Some monocyte, dendritic cell (DC), macrophage, and neutrophil markers are elevated in the 4-1BBL–only group, but less so than many of the lymphocyte markers tested. The general trend seen for lymphocytes was also observable for many of the innate immune cell and general infiltrating leukocyte markers, with slight up-regulation in tumors treated with 4-1BBL, greater up-regulation in tumors treated with IL-12, and the greatest effect in tumors treated with both. However, the difference among groups was most striking for lymphocyte markers, particularly *CD3ε* (T cells) and *CD8a* ($CD8^+$ T cells) and IFN-γ as an activation marker. The data further support the proposed mechanism of action as it highlights that a major effect of the treatment is on the recruitment, activation, and/or expansion of cytotoxic T lymphocytes as the technology was designed to target.

The messenger RNA (mRNA) expression results were also verified by flow cytometry, which yielded similar trends. Tumors were excised 14 d after inoculation (3 d after the final treatment), and groups treated with 4-1BBL, IL-12, or 4-1BBL/IL-12 nanoparticles along with anti–PD-1 showed a higher proportion of tumor-infiltrating lymphocytes (TILs) in the tumor, a greater proportion of which were T cells (Fig. 5 *A* and *B*). Those groups, especially the 4-1BBL/IL-12 nanoparticle group, had the highest proportion of $CD8^+$ cells among the $CD3^+$ T cells, as well as the highest proportion of NK cells among $CD3^-$ TILs (Fig. 5 *C*–*F*). While the $CD4^+$ T cell population was elevated in some of the nanoparticle-treated groups, the proportion of $Foxp3^+$ cells (Tregs) was highest in the 4-1BBL only nanoparticle group, concurring with qPCR results (Fig. 5 *G* and *H*). Interestingly, the effect of checkpoint blockade therapy was clearer in the flow cytometry results where mice treated with only 4-1BBL/IL-12 nanoparticles but no anti–PD-1 showed fewer TILs, T cells, and cytotoxic cells than mice treated with both nanoparticles and anti–PD-1. Immunohistochemistry on the 14-d tumors qualitatively supports the flow cytometry and qPCR results, with CD8 expression showing the presence of cytotoxic T cells throughout the tumor and CD31 expression and LYVE-1 expression showing the presence of blood vessels and lymphatic vessels throughout the tumor (*SI Appendix*, Fig. S7).

After 18 d, significantly more TILs were still present in the group treated with 4-1BBL/IL-12 nanoparticles and anti–PD-1. The proportion of $CD8^+$ cells among total T cells and the ratio of $CD8^+/CD4^+$ T cells were still higher in groups treated with signal 3 or signal 2/3 nanoparticles although fewer of these differences were statistically significant than at 14 d (Fig. 6*A*). The prevalence of Tregs in the 4-1BBL–only nanoparticle-treated group remained high at 18 d, with the spread in the data showing variability of response within the group (Fig. 6*B*). Some of the greater variation at this time point may be due to the large differences in the size of the tumors. Tumors in the group treated with control nanoparticles, control nanoparticles and anti–PD-1, and 4-1BBL nanoparticles and anti–PD-1 had average masses of 700 ± 200 mg, 730 ± 50 mg, and 500 ± 200 mg, respectively (mean ± SE), and some of these tumors had grown large enough to require euthanasia of the mouse (Fig. 6*C*). By contrast, mice treated with 4-1BBL/IL-12 nanoparticles and anti–PD-1 all had significantly smaller tumors (40 ± 20 mg), with relatively few cells that could be extracted for analysis. Other details of flow cytometry analysis are provided in *SI Appendix*, Fig. S6.

Long-Term and Systemic Immunity Conferred by tAPC Nanoparticle Treatment. Some of the mice treated with either 4-1BBL or 4-1BBL/IL-12 nanoparticles and anti–PD-1 fully cleared their tumors and were considered long-term survivors when no disease was detectable after 50 d (twofold longer survival than the longest surviving mouse in the control group) (Fig. 3*C*). At t = 66 d posttumor implantation, the long-term survivors were rechallenged with s.c. B16-F10 melanoma tumors on the opposite flank, along with age-matched, previously untreated controls. The tumor growth rate was significantly slower ($P < 0.0001$ after t = 15 d postchallenge) in the survivors than in controls (Fig. 6*A*). Although all mice did eventually grow tumors in the absence of any further treatment, the long-term survivors lived significantly longer ($P = 0.0089$) than the age-matched controls (Fig. 6*B*), with >100% improvement in median survival time. The ability of these pretreated mice to resist the formation of a new tumor months later, particularly a tumor at a different location, is indicative of a long-lasting and systemic antitumor immune response.

Of the long-term survivors, some developed a depigmented patch of fur on the flank where the original tumor had been implanted and then treated by local nanoparticle injection. This vitiligo-like pattern not only lasted throughout the course of the study but also began to spread to other patches of fur (Fig. 6*C*). Although this was an unintended side effect, the development of vitiligo has been found to correlate with positive responses to immunotherapy in human melanoma patients (40) and is another indication of a cytotoxic immune response specific to melanocytes, the cell type from which the cancer is derived. The later spread of depigmented patches on the mouse is also another indication that

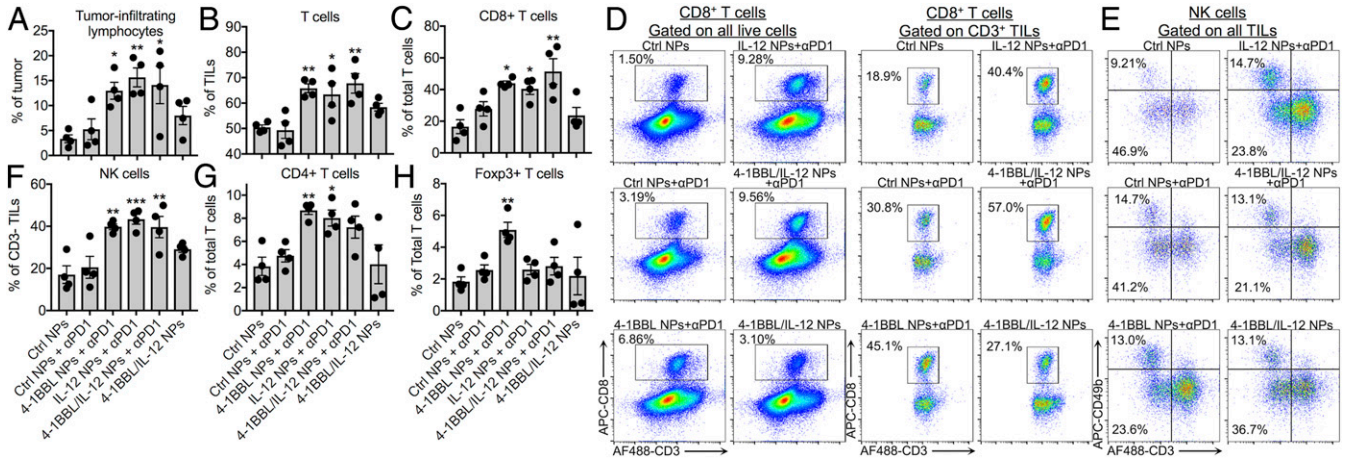

Fig. 5. Flow cytometry after 14 d confirms a cytotoxic immune response in the tumor microenvironment due to tAPC reprogramming NPs. (*A* and *B*) Mice treated with reprogramming nanoparticles, particularly in combination with anti–PD-1, had more TILs and, within TILs, more T cells. (*C* and *D*) tAPC reprogramming resulted in a more $CD8^+$ cytotoxic T cells after 14 d. (*E* and *F*) Among $CD3^-$ TILs, the NK cell population was greater in tAPC-reprogrammed tumors. (*G* and *H*) The $CD4^+$ population was significantly greater among T cells in tAPC-treated tumors, but the $Foxp3^+$ population was not increased in tumors injected with signal 3 or signal 2/3 nanoparticles. Signal 2 nanoparticles in combination with anti–PD-1 did increase the $Foxp3^+$ population. $^*P < 0.05$; $^{**}P < 0.01$; $^{***}P < 0.001$; statistically significant differences were measured by one-way ANOVA with Dunnett posttests comparing to the control (Ctrl NPs). For all bar graphs, mean ± SE of four ($n = 4$) replicates is shown.

the cellular immune response to tAPC reprogramming treatment was not confined to the location where the nanoparticles were locally injected but rather had a systemic component, and the destruction of melanocytes further supports the role of cytotoxic T cells in the antimelanoma response. This finding was further evaluated by dissociating the spleens of tumor-bearing mice treated with either control nanoparticles with or without anti–PD-1 or reprogramming nanoparticles with anti–PD-1.

Splenic $CD8^+$ T cells were isolated and cocultured with 4-1BBL/IL-12-transfected tumor cells in vitro to test for stimulation. We found that $CD8^+$ T cells from spleens of tAPC-treated mice were more activated by transfected B16-F10 cells in vitro, as measured by IFN-γ secretion (Fig. 6*D*). This indicates that splenic $CD8^+$ T cells from tAPC-treated mice were either 1) generally more activated than $CD8^+$ T cells from control mice or 2) enriched for tumor-specific T cells. Interestingly, although these T cells were slightly more activated by transfected MC38

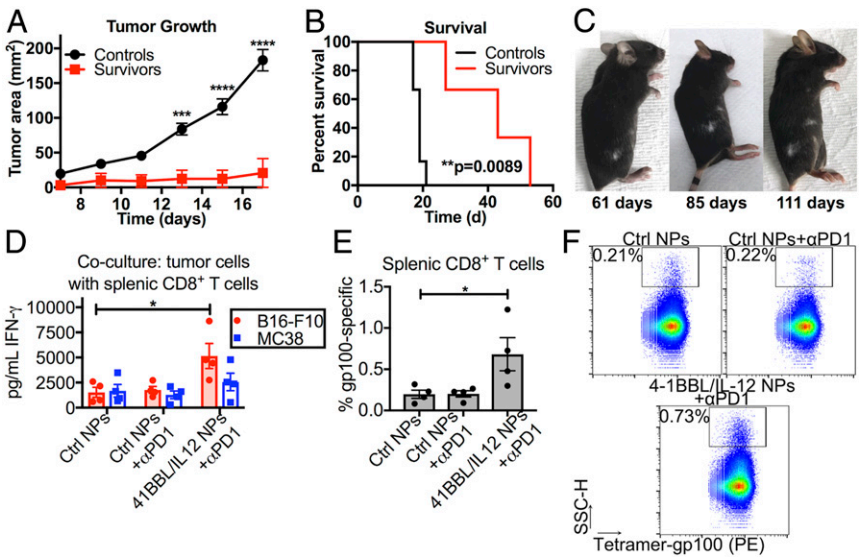

Fig. 6. Local tAPC reprogramming leads to a durable and systemic antitumor immune response. (*A*) Survivors rechallenged with new s.c. B16-F10 tumors on the opposite flank resisted tumor formation compared to untreated control mice and (*B*) survived significantly longer after rechallenge. $^{**}P < 0.01$; $^{***}P < 0.001$; $^{****}P < 0.0001$. (*C*) One of the long-term survivors developed a vitiligo-like patch of depigmented fur at the site of the eliminated tumor, which began to spread to other patches of fur, indicating a cytotoxic immune response at more distant locations. Statistically significant differences in the growth rate were measured by two-way repeated-measures *t* tests with Holm–Sidak tests to correct for multiple comparisons. Differences in survival were calculated by the Mantel–Cox log-rank test. (*D*) $CD8^+$ T cells isolated from tAPC-treated tumor-bearing mice were activated more effectively after in vitro stimulation with B16-F10 cells than $CD8^+$ T cells from tumor-bearing mice administered control nanoparticles or checkpoint inhibition alone. (*E* and *F*) The splenic $CD8^+$ T cell population was more specific for gp100, a common melanoma antigen. PE, phycoerythrin. The graphs show mean ± SE. Significance was calculated by one-way ANOVA with Dunnett posttests against the "Ctrl NPs" group. $^*P < 0.05$.

cells compared to controls, this difference was not statistically significant. This suggests that the T cell response to B16-F10 cells is tumor-specific although there may be some shared epitopes with other tumor cell lines that cause a slight enhancement to the immune response to the other tumor cell line.

The same $CD8^+$ T cells were stained with a tetramer loaded with gp100, a common B16-F10 tumor antigen. Once again, cells isolated from animals treated with tAPC-reprogramming NPs had a higher proportion of gp100-specific T cells (Fig. 6 *E* and *F*). It should be noted that the tAPC reprogramming strategy is not antigen-specific and is expected to generate an immune response directed against various different B16-F10 antigens so the data on only one particular antigen, gp100, while already encouraging, is likely to be an underestimation of the full effects of the treatment. Moreover, although the nanoparticle treatment is administered intratumorally, the effects on $CD8^+$ T cells were measured in the spleen, showing that the antitumor cellular immune response is likely to be widespread in the body and not confined to the initial tumor and nanoparticle injection site.

Applicability of the tAPC Strategy to Other Tumor Types. To support our hypothesis that this tumor reprogramming immunotherapy can have broad clinical applicability, we evaluated this treatment on the MC38 colorectal carcinoma tumor model. We used the same screening methods to identify leading PBAEs for MC38 transfection in vitro and in vivo after i.t. injection into an s.c. tumor (Fig. 7*A*). MC38 cells were transfected with *4-1BBL*, *IL-12*, or both and cocultured with primary splenocytes, and the same trends in IFN-γ secretion were seen with MC38 as with B16-F10 after 1 to 3 d of coculture (Fig. 7*B*). We then carried out an antitumor efficacy study in MC38-bearing mice, and we also showed that treatment with the nanoparticles was effective in slowing or preventing tumor growth (Fig. 7*C*). Excitingly, in this model, all mice in the group treated with 4-1BBL/IL-12 nanoparticles i.t. and anti–PD-1 antibody i.p. survived and fully cleared the initial tumor. Mice treated with 4-1BBL/IL-12 nanoparticles without anti–PD-1 also survived statistically significantly more than mice treated with control nanoparticles without anti–PD-1 (Fig. 7*D*). After 66 d, surviving mice were rechallenged with a second MC38 tumor injected s.c. on the opposite flank, along with naive, age-matched control mice that had not received a first tumor or any treatment. While almost 90% of control mice died due to tumor growth, none of the mice that had survived the first tumor developed the second tumor, indicating a very strong, long-lasting antitumor response at a site distant from the original treatment site.

Discussion

Despite promising preclinical and clinical results of cancer immunotherapy, further research and development are still needed to improve the efficacy and safety of such treatments and to decrease their cost and regulatory burden. Here, we utilized the challenging B16-F10 mouse melanoma model to demonstrate the therapeutic potential of a nonviral nanomedicine that can deliver immunostimulatory genes to a tumor and were able to achieve similarly strong results in a second murine model using MC38 colorectal carcinoma. Given our route of nanoparticle administration (i.t.), the focus of this technology is on solid tumors. In particular, this type of strategy could find clinical use in patients with solid tumors who have lesions that are accessible by needle or catheter but not easily operable. Additionally, we have shown that local nanoparticle delivery leads to a systemic and durable response, which may provide a method of harnessing the immune system to target metastases or invading malignant cells. In this approach, an endogenous cellular response is engendered without requiring ex vivo cellular manipulation.

In contrast to other work describing the delivery of immunostimulatory agents to elicit an antitumor response (21–27), we showed that coexpression of both signals 2 and 3 by signal 1-expressing tumor cells could cause activation of T cells in the direct context of tumor antigens. Thus, while this technology itself is independent of prior knowledge of tumor antigen expression profiles or MHC haplotype, it could activate an immune response specific to the patient and the tumor. Through antitumor efficacy studies, as well as analysis of immune cells in the tumor microenvironment, we have shown that tAPC genetic reprogramming induces a cytotoxic, cell-mediated anticancer response. Not only were some of the treated animals able to clear their tumors, but they also resisted formation of new tumors at a distant location.

Other studies have shown that tumor cells transfected ex vivo to express signals 2 and/or 3 are rejected by immunocompetent mice and lead to protective immunity (41–44), but the need for ex vivo cellular manipulation is a practical hurdle to this type of vaccination that dramatically reduced its accessibility. In contrast, PBAE/DNA nanoparticles can be an off-the-shelf therapy,

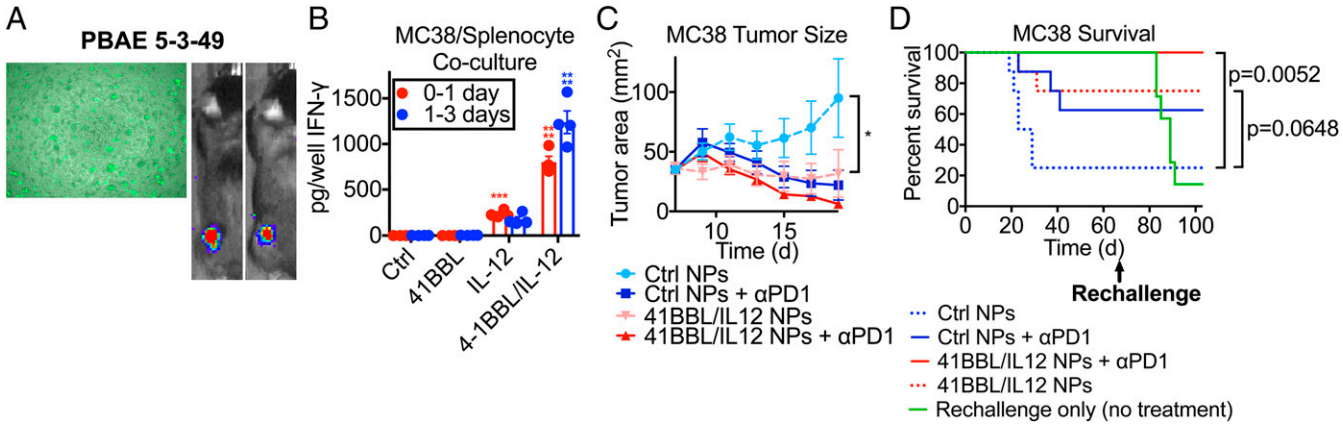

Fig. 7. The tAPC strategy is effective in multiple tumor models. (*A*) MC38 cells could be transfected in vitro and in vivo after i.t. injection with nanoparticles. (*B*) Transfected MC38 cells show the same trends in activating splenocytes as B16-F10 cells, with a synergistic effect seen between signals 2 and 3. For each time point (red and blue), one-way ANOVA was done with Dunnett posttests comparing to "Ctrl." ***$P < 0.001$, ****$P < 0.0001$. (*C*) MC38 tumors grew more slowly after tAPC nanoparticle treatment. Statistically significant differences in the growth rate were measured by two-way repeated-measures *t* tests with Holm–Sidak tests to correct for multiple comparisons. *$P < 0.05$. (*D*) 41BBL/IL12 NPs + αPD1-treated mice survived significantly longer than control NPs + αPD1-treated mice and are also able to 100% reject a rechallenge of the tumor on the opposite flank. Differences in survival were calculated by the Mantel–Cox log-rank test with Bonferroni correction for multiple comparisons.

able to provide a personalized endogenous cellular therapy response via a simple injection. Using PBAEs as DNA-delivery agents, we are able to achieve strong in situ transfection of tumor cells using variants of materials that are safe and specific for cancer cells over healthy tissue (33, 34), thus preventing off-target activation of the immune system against healthy cells. PBAE-based nanoparticles for *4-1BBL* and *IL-12* transfection, therefore, can provide a safe, noninvasive, and easily manufactured technology for generating a potent therapeutic effect against tumors.

This polymeric DNA nanoparticle system brings with it several advantages. While virus-mediated gene delivery can be highly effective (32), their clinical use is hampered by their intrinsic immunogenicity, which can attenuate their activity and also lead to adverse side effects. They are also difficult to manufacture at scale, and their cargo capacity is limited, which may preclude the codelivery of multiple genes within the same particle. Other types of delivery vehicles, such as lipid nanoparticles (LNPs), are often constrained by high toxicity (35) or their own intrinsic immunogenicity, even without nucleic acid cargo (36). Aside from their ability to transfect cancer cells (33, 34, 37, 45, 46), PBAE nanoparticles can deliver dozens of plasmids within the same particle (47, 48). This makes them ideal for the tAPC genetic reprogramming strategy as we have shown here that signals 2 and 3 act synergistically on immune stimulation (Fig. 2). In particular, Figs. 4 and 5 demonstrate the importance of including both signals 2 and 3 in the treatment strategy as the combination of both not only led to the greatest effect but also decreased the chance of inadvertently stimulating undesirable cell types like Tregs. The presentation of surface-bound 4-1BBL signal 2 on malignant cells, ideally coexpressed alongside signal 1 antigens, focuses the immune response at the tumor site while the secretion of the IL-12 signal 3 helps to ensure a Th1 bias. The importance of this coexpression is particularly apparent in the results pertaining to mice treated with *4-1BBL* nanoparticles in the absence of DNA encoding *IL-12*. While treatment with *4-1BBL* alone was effective in some animals, in other mice, the tumor followed the same growth pattern as controls (Fig. 3) and even seemed to contain a higher proportion of $Foxp3^+$ Tregs among TILs (Fig. 5 and *SI Appendix*, Fig. S5). Because 4-1BBL can signal to Tregs, as well as $CD8^+$ T cells, it is possible that overexpression of this signal 2 alone can stimulate an unwanted tolerogenic response rather than the desired cytotoxic antitumor response in some of the animals, which can be avoided with the codelivery of a cytokine like IL-12 that biases the immune system toward a Th1 antitumor response.

The ease of combinatorial design of these particles, demonstrated in Fig. 1 and *SI Appendix*, Fig. S1, and multiple previous reports (33, 34, 37, 47), also imparts flexibility in the chemical properties of the polymer, the genes encoded by the DNA, and the association of polymer and DNA. While the signal 2 costimulatory molecule 4-1BBL and signal 3 cytokine IL-12 were found to be effective in this study, the PBAE/DNA nanotechnology provides a platform in which different polymers, as well as other immunostimulatory genes, can be easily used in a modular manner. While other nucleic acid delivery technologies have recently been described for use as immunotherapies (49), the underlying premise of which is supported by our findings, the use of plasmid DNA here rather than mRNA allows greater cargo stability and a simpler and less expensive manufacturing process, increasing the translatability of this work. Critically, a patient-specific response is engendered without requiring a priori knowledge of a patient's target antigens or ex vivo manipulation of a patient's cells. Finally, the ability of PBAE/DNA nanoparticles to be assembled in a simple protocol, be easily scalable (48), and to be stored in a stable form for at least 2 y (34) further supports the translational potential of this biotechnology and its possible broad impact on cancer patients.

Materials and Methods

Poly(Beta-Amino Ester) Synthesis. PBAEs were synthesized according to the reaction scheme in Fig. 1*A* as previously described (33), with each polymer consisting of one diacrylate "backbone" monomer (B), one aminoalcohol "sidechain" monomer (S), and one amine-terminated "end-cap" monomer (E). Final PBAEs are named by a series of three hyphenated numerals, corresponding to the backbone, sidechain, and end-cap used in their synthesis.

In Vitro Transfection of Cells: Screening with Reporter Gene. B16-F10 murine melanoma cells and MC38 murine colorectal cancer cells were a kind gift from Jonathan P. Schneck, Johns Hopkins University, Baltimore, MD. Both cell lines were cultured in complete growth medium consisting of RPMI 1640 (Gibco) supplemented with 10% fetal bovine serum (FBS) and 1% penicillin/streptomycin and were maintained at <80% confluency. The day before the transfection, cells were seeded in flat-bottom 96-well plates at 5×10^4 cells per well in 100 μL of complete growth medium. On the day of transfection, nanoparticles were formed by diluting both green fluorescent protein (GFP) plasmid DNA (pEGFP-N1, purchased from Clontech and amplified by Elim Biopharmaceuticals [Hayward, CA]) and an array of PBAE polymers in 25 mM sodium acetate buffer, pH 5 (NaAc) and then mixing the diluted DNA and PBAEs to allow self-assembly. After 10 min, nanoparticles were added to the cells in complete growth medium at a final DNA concentration of 5 μg/mL and final PBAE concentrations ranging from 150 to 450 μg/mL The cells were incubated with nanoparticles at 37 °C and 5% CO_2 for 2 h, and then the media were replaced with 100 μL of fresh complete growth medium per well.

To assess toxicity of the PBAE/DNA nanoparticles, an MTS assay was carried out 24 h after transfection (CellTiter 96 Aqueous One Solution Cell Proliferation Assay, Promega, Madison, WI) to measure the metabolic activity of B16-F10 or MC38 cells. Transfection efficacy was assessed by flow cytometry 48 h after transfection, using an Accuri C6 flow cytometer (BD Biosciences, San Jose, CA) with a Hypercyt high-throughput attachment (IntelliCyt, Albuquerque, NM) and 1× phosphate-buffered saline (PBS) with 2% FBS as buffer. Transfection was measured as the percentage of total cells per well that were GFP^+ as well as by geometric mean GFP fluorescence intensity. For both toxicity and transfection assays, PBAE/DNA nanoparticle-treated cells were compared to untreated cells as a control.

In Vivo Transfection of Tumors: Selection of PBAE Formulation Using Reporter Gene. All animal work described here was carried out in accordance with the guidelines set by the Johns Hopkins Animal Care and Use Committee. To select the top PBAE formulation, subcutaneous (s.c.) tumors were transfected with firefly luciferase (fLuc; pcDNA3-fLuc plasmid amplified by Aldevron, Fargo, ND) via intratumoral (i.t.) nanoparticle injection. The flanks of female C57BL/6J mice (The Jackson Laboratory, Bar Harbor, ME) were shaved. Under anesthesia by isoflurane inhalation, 3×10^5 B16-F10 cells in basal RPMI medium (without serum or antibiotics) were injected s.c. into each flank in 100 μL volume. For studies in MC38-bearing mice, tumors were established by shaving the flanks of mice and injecting 5×10^5 cells s.c. into each flank in 100 μL of basal RPMI medium. After 7 d, when tumors had become palpable, mice were again anesthetized under isoflurane. PBAE/DNA nanoparticles were formed as described above using sodium acetate buffer at pH 7 to prevent excessive acidification of the tissue environment and injected i.t. in 25 μL volume. Due to the increased concentration, nanoparticles were all tested at a 30:1 wt/wt ratio of polymer to DNA, with a final DNA dose of 5 μg per tumor. Each tumor was considered a separate replicate. After 24 h, mice were injected intraperitoneally (i.p.) with 150 mg/kg d-luciferin (potassium salt solution in 1× PBS; Cayman Chemical Company, Ann Arbor, MI). After 8 min, mice were imaged by the In Vivo Imaging System (IVIS Spectrum; PerkinElmer, Shelton, CT) to measure bioluminescence. All mice were euthanized before the combined tumor area of both tumors exceeded 200 mm^2 measured by calipers. The nanoparticle formulation leading to the highest fLuc bioluminescence signal in both tumor models, PBAE 5-3-49 at 30 wt/wt mass ratio to DNA, was used for all future in vivo studies.

In Vitro T and NK Cell Stimulation by Transfected B16-F10 Cells. B16-F10 cells were seeded in 96-well plates and transfected as described above with PBAE/DNA nanoparticles encoding fLuc (control), 4-1BBL, IL-12, or a mixture of 4-1BBL and IL-12 at a 1:1 plasmid mass ratio. The next day, 8- to 12-wk-old female C57BL/6J mice were euthanized by CO_2 asphyxiation. Their spleens were removed and dissociated by pressing through a 40-μm cell strainer and washing with excess cold 1× PBS. The cells were pelleted by centrifugation at 300 relative centrifugal force for 5 min at 4 °C, and the supernatant was removed. Red blood cells were lysed by resuspending the pellet in 1 mL of

ACK lysing buffer (Quality Biological, Gaithersburg, MD) for 1 min at room temperature, then diluting in 10 mL of cold 1× PBS. The cell suspension was centrifuged again at 300 rcf for 5 min at 4 °C, the supernatant was removed, and the pellet was resuspended in MACS running buffer (1× PBS with 0.5% bovine serum albumin [BSA] and 2 mM EDTA). Cells were labeled with microbeads for magnetic negative isolation of $CD8^+$ T cells or NK cells according to the manufacturer's instructions (Miltenyi Biotec, Auburn, CA) using MACS separation columns.

The isolated $CD8^+$ T cells or NK cells were then resuspended at 2×10^6 cells per milliliter in complete RPMI growth medium and added directly to the plate of transfected B16-F10 cells (10^5 lymphocytes in 50 μL added per well). After 18 h of incubation at 37 °C and 5% CO_2, the media in the wells were collected and measured by IFN-gamma (IFN-γ) ELISA (mouse IFN gamma uncoated ELISA; Invitrogen/Thermo Fisher Scientific, Carlsbad, CA).

Differences in IFN-γ secretion among groups were detected by one-way ANOVA with Dunnett posttests against the control (tumor cells transfected with fLuc control plasmid and cocultured with T or NK cells). Differences were considered statistically significant for $P < 0.05$.

In Vivo Antitumor Efficacy of tAPC Reprogramming Nanoparticles in B16-F10 Model. Female 9-wk-old C57BL/6J mice were inoculated s.c. with 3×10^5 B16-F10 cells on the right flank following the procedures described above. After 7 d, the area (width × length) of each tumor was measured by caliper, and the animals were ranked according to tumor size. Mice were assigned to each group, ensuring that all groups started with statistically equivalent mean tumor sizes. The experimenter administering treatments and measuring tumor size over time was blinded to group assignments.

On days 7, 9, and 11 after tumor inoculation, PBAE nanoparticles with DNA encoding fLuc (control), 4-1BBL, IL-12, or a 1:1 mixture of 4-1BBL and IL-12 were injected i.t., with a final DNA dose of 5 μg in 25 μL per injection, as described above. On days 7 and 9, mice were also injected i.p. with 200 μg and 100 μg of monoclonal antibody against mouse PD-1, respectively (clone RMP1-14; BioXCell, West Lebanon, NH) or 1× PBS alone as a control. Tumor area was measured every 2 d after the start of treatment, and mice were euthanized when tumor area reached or exceeded 200 mm^2. Each group included $n = 7$ mice. Differences in tumor size over time among mice treated with nanoparticles and anti–PD-1 were detected by two-way repeated-measures ANOVA with Dunnett posttests against the control group (control fLuc nanoparticles administered i.t. and anti–PD-1 administered i.p.). Differences were considered statistically significant for $P < 0.05$.

Mice that cleared their tumor and survived with no apparent disease to t = 50 d (two-old greater survival time than the last surviving mouse in the control group) were considered long-term survivors. Long-term survivors were rechallenged on the opposite (left) flank with an injection of 3×10^5 B16-F10 cells at t = 66 d following the initial tumor inoculation following the procedures described above. Naive, untreated, age-matched (18-wk-old) female C57BL/6J mice were inoculated with the same number of B16-F10 cells at the same time as controls. No further treatment was administered to any of the mice. Tumor size was measured over time by caliper, and survival was recorded. Differences in tumor size over time between the two groups were detected by *t* tests with Holm–Sidak corrections for multiple comparisons. Differences were considered statistically significant for $P < 0.05$. Differences in survival curves were detected by Mantel–Cox log-rank tests, with a Bonferroni correction for multiple comparisons.

Statistics. Unless otherwise specified, differences between two groups were calculated using Student's *t* tests, with Holm–Sidak corrections for multiple comparisons where necessary. Differences among multiple groups at a single time point were calculated using one-way ANOVAs with Dunnett posttests against the control group specified in each section above. Differences among multiple groups across multiple time points were calculated using two-way repeated-measures ANOVAs with Dunnett posttests against the control group. The normality of data distributions was verified by Shapiro–Wilk tests.

Data Availability. All data are contained in the manuscript text and *SI Appendix*. The data in other formats is also available upon request from the corresponding author.

ACKNOWLEDGMENTS. This work was supported by National Institutes of Health Grants R01CA228133 and P41EB028239. We thank Prof. Joshua Doloff (Johns Hopkins University) for advice on immunological analysis.

1. J. M. Redman, G. T. Gibney, M. B. Atkins, Advances in immunotherapy for melanoma. *BMC Med.* **14**, 20 (2016).
2. I. Mellman, G. Coukos, G. Dranoff, Cancer immunotherapy comes of age. *Nature* **480**, 480–489 (2011).
3. E. Ben-Akiva, R. A. Meyer, D. R. Wilson, J. J. Green, Surface engineering for lymphocyte programming. *Adv. Drug Deliv. Rev.* **114**, 102–115 (2017).
4. J. M. Curtsinger *et al.*, Inflammatory cytokines provide a third signal for activation of naive CD4+ and CD8+ T cells. *J. Immunol.* **162**, 3256–3262 (1999).
5. J. Banchereau, A. K. Palucka, Dendritic cells as therapeutic vaccines against cancer. *Nat. Rev. Immunol.* **5**, 296–306 (2005).
6. P. W. Kantoff *et al.*; IMPACT Study Investigators, Sipuleucel-T immunotherapy for castration-resistant prostate cancer. *N. Engl. J. Med.* **363**, 411–422 (2010).
7. S. Anguille, E. L. Smits, E. Lion, V. F. van Tendeloo, Z. N. Berneman, Clinical use of dendritic cells for cancer therapy. *Lancet Oncol.* **15**, e257–e267 (2014).
8. P. J. Tacken, I. J. M. de Vries, R. Torensma, C. G. Figdor, Dendritic-cell immunotherapy: From ex vivo loading to in vivo targeting. *Nat. Rev. Immunol.* **7**, 790–802 (2007).
9. C. Wang, W. Sun, Y. Ye, H. N. Bomba, Z. Gu, Bioengineering of artificial antigen presenting cells and lymphoid organs. *Theranostics* **7**, 3504–3516 (2017).
10. L. J. Eggermont, L. E. Paulis, J. Tel, C. G. Figdor, Towards efficient cancer immunotherapy: Advances in developing artificial antigen-presenting cells. *Trends Biotechnol.* **32**, 456–465 (2014).
11. R. F. Wang, H. Y. Wang, Immune targets and neoantigens for cancer immunotherapy and precision medicine. *Cell Res.* **27**, 11–37 (2017).
12. K. Shi, M. Haynes, L. Huang, Nanovaccines for remodeling the suppressive tumor microenvironment: New horizons in cancer immunotherapy. *Front. Chem. Sci. Eng.* **11**, 676–684 (2017).
13. D. S. Chen, I. Mellman, Oncology meets immunology: The cancer-immunity cycle. *Immunity* **39**, 1–10 (2013).
14. J. D. Comber, R. Philip, MHC class I antigen presentation and implications for developing a new generation of therapeutic vaccines. *Ther. Adv. Vaccines* **2**, 77–89 (2014).
15. H. Zhang *et al.*, 4-1BB is superior to CD28 costimulation for generating CD8+ cytotoxic lymphocytes for adoptive immunotherapy. *J. Immunol.* **179**, 4910–4918 (2007).
16. J. A. Chacon *et al.*, Co-stimulation through 4-1BB/CD137 improves the expansion and function of CD8(+) melanoma tumor-infiltrating lymphocytes for adoptive T-cell therapy. *PLoS One* **8**, e60031 (2013).
17. M. Xu *et al.*, Regulation of antitumor immune responses by the IL-12 family cytokines, IL-12, IL-23, and IL-27. *Clin. Dev. Immunol.* **2010**, 832454 (2010).
18. J. Ni, M. Miller, A. Stojanovic, N. Garbi, A. Cerwenka, Sustained effector function of IL-12/15/18-preactivated NK cells against established tumors. *J. Exp. Med.* **209**, 2351–2365 (2012).
19. T. Bartkowiak, M. A. Curran, 4-1BB agonists: Multi-potent potentiators of tumor immunity. *Front. Oncol.* **5**, 117 (2015).
20. J. Hsu *et al.*, Contribution of NK cells to immunotherapy mediated by PD-1/PD-L1 blockade. *J. Clin. Invest.* **128**, 4654–4668 (2018).
21. P. C. Emtage *et al.*, Adenoviral vectors expressing lymphotactin and interleukin 2 or lymphotactin and interleukin 12 synergize to facilitate tumor regression in murine breast cancer models. *Hum. Gene Ther.* **10**, 697–709 (1999).
22. I. Narvaiza *et al.*, Intratumoral coinjection of two adenoviruses, one encoding the chemokine IFN-gamma-inducible protein-10 and another encoding IL-12, results in marked antitumoral synergy. *J. Immunol.* **164**, 3112–3122 (2000).
23. T. Nomura, H. Hasegawa, M. Kohno, M. Sasaki, S. Fujita, Enhancement of anti-tumor immunity by tumor cells transfected with the secondary lymphoid tissue chemokine EBI-1-ligand chemokine and stromal cell-derived factor-1alpha chemokine genes. *Int. J. Cancer* **91**, 597–606 (2001).
24. Y. Fan *et al.*, Immunogenic cell death amplified by co-localized adjuvant delivery for cancer immunotherapy. *Nano Lett.* **17**, 7387–7393 (2017).
25. M. C. Hanson *et al.*, Nanoparticulate STING agonists are potent lymph node-targeted vaccine adjuvants. *J. Clin. Invest.* **125**, 2532–2546 (2015).
26. N. Cheng *et al.*, A nanoparticle-incorporated STING activator enhances antitumor immunity in PD-L1-insensitive models of triple-negative breast cancer. *JCI Insight* **3**, 120638 (2018).
27. G. Zhu *et al.*, Intertwining DNA-RNA nanocapsules loaded with tumor neoantigens as synergistic nanovaccines for cancer immunotherapy. *Nat. Commun.* **8**, 1482 (2017).
28. W. Lasek, R. Zagożdżon, M. Jakobisiak, Interleukin 12: Still a promising candidate for tumor immunotherapy? *Cancer Immunol. Immunother.* **63**, 419–435 (2014).
29. A. M. Di Giacomo, M. Biagioli, M. Maio, The emerging toxicity profiles of anti-CTLA-4 antibodies across clinical indications. *Semin. Oncol.* **37**, 499–507 (2010).
30. J. P. Leonard *et al.*, Effects of single-dose interleukin-12 exposure on interleukin-12-associated toxicity and interferon-gamma production. *Blood* **90**, 2541–2548 (1997).
31. Z. Cheng *et al.*, In vivo expansion and antitumor activity of coinfused CD28- and 4-1BB-engineered CAR-T cells in patients with B cell leukemia. *Mol. Ther.* **26**, 976–985 (2018).
32. C. M. Guenther *et al.*, Synthetic virology: Engineering viruses for gene delivery. *Wiley Interdiscip. Rev. Nanomed. Nanobiotechnol.* **6**, 548–558 (2014).
33. S. Y. Tzeng, L. J. Higgins, M. G. Pomper, J. J. Green, Biomaterial-mediated cancer-specific DNA delivery to liver cell cultures using synthetic poly(beta-amino ester)s. *J. Biomed. Mater. Res. A* **101A**, 1837–1845 (2013).
34. H. Guerrero-Cázares *et al.*, Biodegradable polymeric nanoparticles show high efficacy and specificity at DNA delivery to human glioblastoma in vitro and in vivo. *ACS Nano* **8**, 5141–5153 (2014).

35. H. Y. Xue, S. Liu, H. L. Wong, Nanotoxicity: A key obstacle to clinical translation of siRNA-based nanomedicine. *Nanomedicine (Lond.)* **9**, 295–312 (2014).
36. D. P. Vangasseri *et al*., Immunostimulation of dendritic cells by cationic liposomes. *Mol. Membr. Biol.* **23**, 385–395 (2006).
37. A. Mangraviti *et al*., Polymeric nanoparticles for nonviral gene therapy extend brain tumor survival in vivo. *ACS Nano* **9**, 1236–1249 (2015).
38. C. M. Díaz-Montero *et al*., Priming of naive CD8+ T cells in the presence of IL-12 selectively enhances the survival of CD8+CD62Lhi cells and results in superior anti-tumor activity in a tolerogenic murine model. *Cancer Immunol. Immunother.* **57**, 563–572 (2008).
39. K. Gee, C. Guzzo, N. F. Che Mat, W. Ma, A. Kumar, The IL-12 family of cytokines in infection, inflammation and autoimmune disorders. *Inflamm. Allergy Drug Targets* **8**, 40–52 (2009).
40. Y. Nakamura *et al*., Correlation between vitiligo occurrence and clinical benefit in advanced melanoma patients treated with nivolumab: A multi-institutional retrospective study. *J. Dermatol.* **44**, 117–122 (2017).
41. L. Chen *et al*., Costimulation of antitumor immunity by the B7 counterreceptor for the T lymphocyte molecules CD28 and CTLA-4. *Cell* **71**, 1093–1102 (1992).
42. S. E. Townsend, J. P. Allison, Tumor rejection after direct costimulation of CD8+ T cells by B7-transfected melanoma cells. *Science* **259**, 368–370 (1993).
43. S. Baskar *et al*., Constitutive expression of B7 restores immunogenicity of tumor cells expressing truncated major histocompatibility complex class II molecules. *Proc. Natl. Acad. Sci. U.S.A.* **90**, 5687–5690 (1993).
44. K. Hiroishi, T. Tüting, H. Tahara, M. T. Lotze, Interferon-alpha gene therapy in combination with CD80 transduction reduces tumorigenicity and growth of established tumor in poorly immunogenic tumor models. *Gene Ther.* **6**, 1988–1994 (1999).
45. C. G. Zamboni *et al*., Polymeric nanoparticles as cancer-specific DNA delivery vectors to human hepatocellular carcinoma. *J. Controlled Release* **263**, 18–28 (2017).
46. J. Kim, Y. Kang, S. Y. Tzeng, J. J. Green, Synthesis and application of poly(ethylene glycol)-co-poly(β-amino ester) copolymers for small cell lung cancer gene therapy. *Acta Biomater.* **41**, 293–301 (2016).
47. N. S. Bhise, K. J. Wahlin, D. J. Zack, J. J. Green, Evaluating the potential of poly(beta-amino ester) nanoparticles for reprogramming human fibroblasts to become induced pluripotent stem cells. *Int. J. Nanomedicine* **8**, 4641–4658 (2013).
48. D. R. Wilson *et al*., Continuous microfluidic assembly of biodegradable poly(beta-amino ester)/DNA nanoparticles for enhanced gene delivery. *J. Biomed. Mater. Res. A* **105**, 1813–1825 (2017).
49. S. L. Hewitt *et al*., Durable anticancer immunity from intratumoral administration of IL-23, IL-36γ, and OX40L mRNAs. *Sci. Transl. Med.* **11**, eaat9143 (2019).